Chemical Engineering Science 141 (2016) 293–303

Contents lists available at ScienceDirect

Chemical Engineering Science

journal homepage: www.elsevier.com/locate/ces

Understanding adsorption behavior of silica nanoparticles over a cellulose surface in an aqueous medium

Parul Katiyar [a], Tarak K. Patra [a,1], Jayant K. Singh [a,*], Deboleena Sarkar [b], Amitava Pramanik [b]

[a] Department of Chemical Engineering, Indian Institute of Technology Kanpur, Kanpur 208016, India
[b] Unilever R & D Bangalore, 64 Main Road, Whitefield, Bangalore 560066, India

HIGHLIGHTS

- BD study delineates the mechanism of suspension and adsorption of nanoparticles.
- The electrostatic screening length controls particles' suspension and adsorption.
- Adsorbed particles form a monolayer, independent of their bulk concentration.
- The monolayer is either gas or liquid like, depending on their bulk concentration.

ARTICLE INFO

Article history:
Received 11 June 2015
Received in revised form
25 November 2015
Accepted 26 November 2015
Available online 3 December 2015

Keywords:
Adsorption
Nanoparticle suspension
DLVO theory
Zeta potential
Hamaker constant
Brownian dynamics

ABSTRACT

The suspension and adsorption of silica nanoparticles on a cellulose surface, in an aqueous medium is investigated using Brownian dynamic simulations. The inter particle and particle–surface interactions are modeled within the framework of the DLVO theory. Our analysis predicts the accumulation of negatively charged nanoparticles near a negatively charged surface depending on the Debye screening length of the medium. A crossover from the suspension to the adsorption of negatively charged silica nanoparticles onto a negatively charged cellulose surface has been reported as the screening length (k^{-1}) of the medium increases. The crossover is observed at $k^{-1} = 100$ nm, due to the interplay between the nanoparticle–nanoparticle and the nanoparticle–surface interactions. The adsorption behavior of nanoparticles is explained using the potential of mean force analysis. The amount of nanoparticles adsorbed depends on their bulk volume fraction (ϕ) and the screening length of the medium. Further, the effects of electrical potentials of nanoparticle (Ψ_P) and surface (Ψ_S) on the adsorption are reported. The data suggests that the adsorption of nanoparticles increases either with increasing Ψ_P magnitude, or/and, with decreasing Ψ_S magnitude. The adsorbed particles form a disordered monolayer, and undergo subdiffusive motion. We have also observed a transition from the gas-like structure to the liquid-like structure of nanoparticles in the adsorbed monolayer as their bulk volume fraction increases.

1. Introduction

Adsorption of nanoparticles and their self-assembly on surfaces are common to many fields of engineering such as film manufacturing, coating, and catalysts (Johnson and Lenhoff, 1996; Kasemo et al., 2000; Nakanishi et al., 2001; Nepal et al., 2012; Zhang and Bai, 2002). Self-assembled and ordered structures of adsorbed nanoparticles on a surface are fascinating owing to their unique optical and electronic properties. For example, silica nanoparticles adsorbed on a modified glass substrate finds application in antireflective coatings (Hattori, 2001; Liu and Yeh, 2010). In addition, coatings of various different particles on substrates are used in data storage, sensors (Chaikin et al., 2013; Velev and Kaler, 1999), lithography masks (Hanarp et al., 2003), and template for photonic crystals (Joannopoulos et al., 1995). Adsorption of biomolecules like protein on surfaces are also very useful for biomaterial selection (Jeon et al., 1991), medicines and enzyme-enhanced laundry detergents. The collective properties of adsorbed nanoparticles on a surface are largely dependent on their arrangement. Therefore, in many engineering applications, heterogeneous surfaces are used to control the structure and dynamics of adsorbed particles (Adamczyk et al., 2002, 2005). It is also shown that surfaces pre-covered with smaller particles are very promising candidate for membrane filtration and anti-biofouling (Adamczyk et al., 2001). Similarly, patterned surfaces with grooves or holes are fabricated to generate a large area defect free ordered array of particles

* Corresponding author.
E-mail address: jayantks@iitk.ac.in (J.K. Singh).
[1] Present address: Department of Polymer Engineering, The University of Akron, Akron, OH 44325, United States.

http://dx.doi.org/10.1016/j.ces.2015.11.026
0009-2509/

Nomenclature

A_{pp}	Hamaker constant for the interactions between a pair of nanoparticles, J
A_{ps}	Hamaker constant for the interactions between nanoparticle and surface, J
$A_{Surface}$	Area of a single surface, dimensionless
a	Radius of a nanoparticle, nm
$\overline{a}$	Radius of a nanoparticle, dimensionless
B_{PP}	Yukawa coefficient for particle–particle interaction, dimensionless
B_{PS}	Yukawa coefficient for particle–surface interaction, dimensionless
e	Electronic charge, C
$\overline{F}_C$	Conservative force, dimensionless
$\overline{F}_f$	Frictional drag force, dimensionless
$\overline{F}_r$	Random force, dimensionless
F_f	Frictional drag force, kg m/s^2
F_r	Random force, kg m/s^2
F_{PP}	Force between two nanoparticles, dimensionless
F_{PS}	Force between nanoparticle and surface, dimensionless
$g_{in\text{-}plane}(r)$	2D-radial distribution function, dimensionless
$g_{bulk}(r)$	Radial distribution function of all the particles in the system, dimensionless
h_p	Peak height of a z-density profile, dimensionless
k_B	The Boltzmann constant, J/K
k^{-1}	Screening length, nm
ka	Inverse of screening length, dimensionless
L_X	Simulation box length in x-direction, dimensionless
L_Y	Simulation box length in y-direction, dimensionless
$\overline{m}$	Mass of a nanoparticle, dimensionless
m	Mass of a nanoparticle, kg
MSD	Mean squared displacement, dimensionless
$n(z)$	Number of nanoparticles within a distance between z and $z+\Delta z$ along z direction
N_{box}	Total number of particles in the box
$n_{ad}(\bar{t})$	Number of nanoparticles adsorbed on the surface at time $\bar{t}$
N_{ad}	Total number of nanoparticles adsorbed on the surface
N_m	Total number of nanoparticles in a monolayer
$\langle N(r, r+\Delta r)\rangle$	Average number of particles in a circular bin between two distances r and $r+\Delta r$ from the center of a particle
$\langle N_b(r, r+\Delta r)\rangle$	Average number of particles in a spherical bin between two distances r and $r+\Delta r$ from the center of a particle
PMF_{PP}	Potential of mean force between two particles, dimensionless
PMF_{PS}	Potential of mean force between particle and surface, dimensionless
r	Center to center distance between two particle, dimensionless
$r_i(\bar{t})$	Position vector of a nanoparticle 'i' at a time,$\bar{t}$
Δr	Bin width for $g_{bulk}(r)$ and $g_{in\text{-}plane}(r)$, dimensionless
T	Temperature, K
$\overline{T}$	Temperature, dimensionless
$\bar{t}$	Time, dimensionless
t	Time, s
Δt	Time step, ns
U	Interaction energy, dimensionless
U_{PP}	Interparticle interaction energy, dimensionless
U_{PS}	Particle–surface interaction energy, dimensionless
$U_{EL(PP)}$	Electrostatic interaction energy between two particles, dimensionless
$U_{EL(PS)}$	Electrostatic interaction energy between a particle and the surface, dimensionless
$U^{att}_{LJ(PP)}$	The effective Lennard-Jones attractive interaction energy between two particles, dimensionless
$U^{att}_{LJ(PS)}$	The effective Lennard-Jones attractive interaction energy between particle and surface, dimensionless
$U^{rep}_{LJ(PP)}$	The effective Lennard-Jones repulsive interaction energy between two particles, dimensionless
$U^{rep}_{LJ(PS)}$	The effective Lennard-Jones repulsive interaction energy between particle and surface, dimensionless
V_{box}	Volume of the simulation box, dimensionless
v	Velocity of a particle, m/s
$\overline{v}$	Velocity of a particle, dimensionless
z	Distance between the center of a particle and the surface, dimensionless
Δz	Bin width for ρ_z, dimensionless
Ψ_s	Electrical potential of the surface, mV
Ψ_p	Electrical potential of the nanoparticle, mV
$\overline{\Psi}_S$	Electrical potential of the surface, dimensionless
$\overline{\Psi}_P$	Electrical potentials of the nanoparticle, dimensionless
η	Viscosity of solvent, Pa s
$\theta(\bar{t})$	Surface coverage, dimensionless
θ_{max}	Maximum surface coverage, dimensionless
θ_∞	Surface coverage in infinite time, dimensionless
ε	Dielectric constant of the solution, dimensionless
ε_0	Dielectric permittivity of free space, F/m
ϕ	Bulk volume fraction of nanoparticles, dimensionless
Γ	Damping factor of the medium, s
ρ_z	z-density of nanoparticles, dimensionless
τ_0	Time, ns
σ	Exclusion thickness, dimensionless

over surfaces (Juillerat et al., 2005). Moreover, square shape charged stripes on a surface induce a great degree of order among the adsorbed particles on it (Brewer et al., 2010). In addition to the adsorption of particles and their arrangement over a surface, the suspension of particles in an aqueous medium is also important for many nano-biotechnological applications. For example, proteins, which are present in blood or solution, get adsorbed on an artificial surface to which they are exposed. Hence, minimizing protein adsorption, is important in areas of blood-contacting devices, chromatographic supports, contact lenses, immunoassays, etc. (Jeon and Andrade, 1991; Jeon et al., 1991). Therefore, the behavior of nanoparticles, proteins, viruses and various other macromolecules on surfaces have received considerable research interests in recent years.

Various models have been proposed to properly capture the adsorption of particles over surfaces in last few decades. The earliest one is the random sequential adsorption model (RSA) (Feder, 1980). In this model, particles are individually and randomly placed on a surface such that no particle overlaps with previously placed particles. At a time one particle is placed on the surface, and it remains permanently fixed to its adsorbed position. However, this model does not incorporate some important aspects of the process – such as explicit particle–surface interactions,

interaction among particles, surface diffusion of adsorbed particles etc. Subsequently, the Monte Carlo simulations have been used widely to incorporate some of the practical aspect of adsorption process. The Monte Carlo method is successfully used to predict the adsorption of colloidal particles (Kulkarni et al., 2003) and orientation of antibodies on charged surfaces (Zhou et al., 2004). However, it could not capture the dynamical aspect of the adsorption process. Hence, Brownian dynamic (BD) simulations are being adopted to capture both equilibrium and dynamical properties. In Brownian dynamics simulations, the interaction between nanoparticles can be represented using the DLVO theory. The DLVO theory (Magan and Sureshkumar, 2006) predicts the effective electrostatic and van der Waals pair potentials between particle–particle and surface–particle interactions in a solution. Models based on the DLVO theory have been successfully used to understand the dynamics (Miyahara et al., 2004; Watanabe et al., 2005) and adsorption of lysozyme (Ravichandran and Talbot, 2000) and polystyrene latex on bare mica (Adamczyk et al., 1992) and silanized mica surfaces (Adamczyk and Szyk, 2000), with friction (Watanabe and Miyahara, 2010), and without friction (Miyahara et al., 2006) and various other systems. Thus, many features of the adsorption process are studied within the framework of Brownian dynamics simulations and DLVO theory. This approach is able to explain experimental findings, and has been successful in obtaining a comprehensive picture of the adsorption process.

It has been shown that, in general, the adsorption of nanoparticles at a solid–liquid interface depends on the particle potential, surface potential, volume fraction and the Debye screening length($1/k$). In case of oppositely charged surface and nanoparticles, the particle potential is found to be dominant parameter controlling the final surface coverage. However, the ordering of the adsorbed nanoparticles are mainly determined by the surface potential (Gray and Bonnecaze, 2001). The surface coverage is also found to increase for high ionic strength of solution, which reduces the lateral mobility of the adsorbed nanoparticles. Further, the deposition of nanoparticles on a solid surface is usually irreversible (Adamczyk and Szyk, 2000; Semmler et al., 1998). Adsorbed nanoparticles are confined to a monolayer due to the electrostatic repulsion between the free and deposited particles. The irreversible deposition of nanoparticles are also predicted by multi-scale simulations (Magan and Sureshkumar, 2006) that demonstrated that the surface coverage follows a power law dependence with time at short timescale, and asymptotic behavior at long time-scale.

All the works mentioned above considered the cases where nanoparticles and the surface are oppositely charged. However, a recent experimental work shows that silica nanoparticles get adsorbed on a cellulose surface in an aqueous environment (Mahouche-Chergui et al., 2014). However, in an aqueous medium, both silica particles and cellulose surface are negatively charged. The amount of adsorption, further, depends on the pH of the medium. Therefore, the adsorption in such a like-charge system is surprising. The interactions between such like-charge particles and the surface, which lead to the adsorption of particles on the surface, are not well understood. Interestingly, the attraction between like charged colloidal particles in a solution is observed in few experiments (Crocker and Grier, 1996; Grier, 1998; Larsen and Grier, 1997). For example, the effective interaction between polystyrene sulfate spheres dispersed in water is attractive when they are confined within two glass walls separated by a distance $d < 5\ \mu m$. However, the effective interaction is purely repulsive when the glass separation d is close to 2.6 μm (Crocker and Grier, 1996). Attractive interactions are also seen from the structure and dynamics of metastable crystals of charged latex spheres (Larsen and Grier, 1997). Similarly, spheres confined by a glass wall or by a concentration of other spheres also feel a long-range attraction, and highly charged spheres in very low salt concentrations also favor attraction (Grier, 1998). The attraction between like charged particles is argued to arise due to a non-equilibrium hydrodynamic effect (Squires and Brenner, 2000), abundant charge separation around each particle (Nagornyak et al., 2009), and multivalent ions with different valence requirements for different polyelectrolytes (Butler et al., 2003; Zhou, 2013). However, several numerical studies, which are conducted to estimate the effective interaction between like charge particles, are contradictory. For example, Bowen and Sharif (1999) calculated a long range attractive interactions between two spherical particles in cylindrical pore by solving the nonlinear Poisson–Boltzmann equation. On the other hand, Gray et al. (1999) using similar methodology and geometry, observed absence of attraction among spherical particles, rather they observed that the repulsive interaction among particles reduces as the confinement increases. Thus, in spite of several works, the cause for the long range attractive interaction between like charge particles is not well understood. In addition, the interaction between like charge particles and a stationary surface, which cause adsorption of particles, is not studied extensively.

In this work, we have investigated the suspension and adsorption in a like charge system. In particular, we have studied the adsorption of silica nanoparticles from its aqueous solution onto a cellulose surface. Here, we analyze different interactions in a like-charge system and explain the adsorption behavior in such systems. Interactions in the system are modeled using the DLVO theory. We have systematically investigated the effects of particles bulk volume fraction, surface potential and screening length on the suspension and adsorption of negatively charged nanoparticles onto a negatively charged surface, using Brownian dynamics simulations. We have also studied various parameters that control the density of the adsorbed monolayer, and its structure and dynamics.

The rest of the paper is organized as follows. The details of the model and Brownian dynamic simulations are described in Section 2. Results are presented and discussed in Section 3, followed by the conclusions in Section 4.

2. Model and methods

We have considered a small volume of aqueous suspension of silica nanoparticles bounded by two cellulose surfaces, as shown in Fig. 1. The two surfaces are placed at the edge of the simulation box in the z-direction. The separations between the surfaces in reduced units are 60, 60, 100, 100, 200 and 200 for ka values of 0.5, 0.25, 0.1, 0.08, 0.05 and 0.03, respectively. The simulation box is periodic along the x- and y-directions. The box length in the z-dimension is considered to be significantly large to avoid slit effects (Gallardo et al., 2012) on the nanoparticles distribution. The simulation box contains 500–20,000 nanoparticles depending on their bulk volume fraction. The nanoparticles bulk volume fraction, ϕ is varied from 0.001 to 0.01 in this study. A nanoparticle is modeled as a spherical bead of radius, $a = 10$ nm. The Brownian dynamics of each nanoparticle is expressed by the Langevin equation of motion (Schneider and Stoll, 1978) as

$$\overline{m}\frac{d\overline{v}(\overline{t})}{d\overline{t}} = \overline{F}_C + \overline{F}_f + \overline{F}_r. \quad (1)$$

where $\overline{F}_C$ is the conservative force due to the inter-particle and surface-particle interactions. The F_f is the frictional drag force or the viscous damping in the medium that is proportional to a particle's velocity v. The F_f is calculated as

$$F_f = -mv/\Gamma. \quad (2)$$

Here, m and Γ correspond to the mass of a nanoparticle and the damping factor of the medium, respectively. The damping factor is related to the mass of a nanoparticle and the viscosity of the medium η as

$$\Gamma = \frac{m}{6\pi\eta a}. \tag{3}$$

The system consists of the solution of silica nanoparticles in water. The damping factor is calculated using the viscosity of water and mass of a silica nanoparticle (Lee and Hua, 2010). The parameters are listed in Table 1. The F_r in Eq. (1) represents a random force that maintains the temperature T of the medium. According to the fluctuation dissipation theorem the magnitude of the random force is (Dünweg and Paul, 1991)

$$F_r \propto \sqrt{\frac{k_B T m}{\Delta t \times \Gamma}}. \tag{4}$$

Here, T, Δt, and k_B represent the temperature of the system, integration time step used in simulations, and the Boltzmann constant, respectively. A random number is used to randomize the direction of the force, similar to our previous works (Patra et al., 2015; Patra and Singh, 2014). Throughout the manuscript, a bar on symbols indicates that, they represent reduced dimensionless quantities. The distances, energies and masses are reduced by nanoparticle radius (a), k_BT and mass of a nanoparticle (m), respectively. The method for non-dimensionalising other quantities is same as described in the LAMMPS manual (Plimpton, 1995) by using these three basic quantities.

The conservative force $\overline{F}_C$ as in Eq. (1) is evaluated from a potential model based on the DLVO theory. This comprises of the effective Lennard-Jones and electrostatic interactions. The nanoparticle–nanoparticle and nanoparticle–surface interaction energies are scaled by k_BT to make them dimensionless. The reduced electrostatic energies are given by the following equations (Oberholzer et al., 1997):

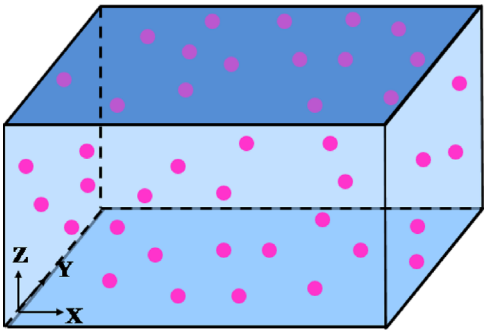

Fig. 1. A schematic representation of the simulation box. The simulation box consists of silica nanoparticles (pink spheres) dispersed in water (blue), bounded by two cellulose surfaces in z-direction (dark blue). (For interpretation of the references to color in this figure legend, the reader is referred to the web version of this article.)

Table 1
Physical parameters used in the simulations.

Physical parameters	Values
a (nm)	10
A_{PP} (zJ) (Senden and Drummond, 1995)	8.4
A_{PS} (zJ) (Bergstrom et al., 1999)	3.5
T (K)	298
ε	78.3
ε_o (pF/m)	8.854
η (Pa s) (Miyahara et al., 2004)	8.94×10^{-4}
e (C)	1.6×10^{-19}

$$U_{EL(PP)}(r) = \frac{B_{PP}}{r}\exp(-ka(r-2)) \tag{5}$$

$$U_{EL(PS)}(z) = B_{PS}\exp(-ka(z-1)) \tag{6}$$

The dimensionless distances r and z denote the center-to-center distance between two nanoparticles and the distance between the surface and the center of a nanoparticle, respectively. Both are obtained after normalizing the actual distances by the nanoparticle radius a. The B_{PP} and B_{PS} are the strength of the nanoparticle–nanoparticle and nanoparticle–surface interactions, respectively. The k corresponds to the inverse Debye screening length. The dimensionless product ka is an important physical parameter that describes the length scale of electrostatic interactions in a medium. The range of k used in this work is based on the pH values measured in an experiment for different concentrations of aqueous silica suspensions (see Supplementary material). The ionic strength of the suspension is due to the dissociation of silanol groups of silica nanoparticles. The k^{-1} is seen to vary from 193 nm to 693 nm in the experiment. Therefore, the simulations are conducted for k^{-1} around this range. Further, the B_{pp} and B_{ps} are derived using far field effective potential for a uniformly charged sphere (Sader, 1997). The B_{PP} and B_{PS} are related to the electric potentials or zeta potential of a nanoparticle and the surface, respectively, as shown in the following equations.

$$B_{PP} = \left(\frac{4\pi k_B T \epsilon \epsilon_o a}{e^2}\right)\left(\frac{\overline{\Psi}_P + 4\gamma\Omega ka}{1+\Omega ka}\right)^2 \tag{7}$$

$$B_{PS} = \left(\frac{4\pi k_B T \epsilon \epsilon_o a}{e^2}\right)\left(\frac{\overline{\Psi}_P + 4\gamma\Omega ka}{1+\Omega ka}\right)\left(4\tan h\left(\frac{\overline{\Psi}_S}{4}\right)\right) \tag{8}$$

where γ and Ω are related to the nanoparticle zeta potential as

$$\gamma = \tan h\left(\frac{\overline{\Psi}_P}{4}\right) \tag{9}$$

$$\Omega = \frac{\overline{\Psi}_P - 4\gamma}{2\gamma^3}. \tag{10}$$

In the above equations, $\overline{\Psi}_S$ and $\overline{\Psi}_P$ are the dimensionless electrical potentials or zeta potentials of the surface and a nanoparticle, respectively. They are obtained after scaling of the actual potentials Ψ_s and Ψ_p by k_BT/e. Eqs. (5) and (6) are valid for all the values of ka and maintain a good accuracy for all surface potentials less than 200 mV (Sader, 1997). The zeta potential of the silica–cellulose system is reported to vary from −50 mV to −10 mV in recent experimental studies, depending on the pH of the medium (Mahouche-Chergui et al., 2014). Thus, simulations are conducted for different combinations of Ψ_P and Ψ_S within this range, as listed in Table 2.

Now, we discuss the effective Lennard-Jones interaction in the system. The attractive part of the effective Lennard-Jones (Hamaker, 1937; Oberholzer et al., 1997) interaction energies for

Table 2
Different combinations of the nanoparticle and surface zeta potential values, used for studying the adsorption behavior of the nanoparticles on the surface at different ka values ranging from 0.03 to 0.1.

	Ψ_P (mV)	Ψ_S (mV)
1	−35	−12, −8, −4
2	−40	−12, −8, −4
3	−45	−12, −8, −4
4	−50	−12, −8, −4
5	−55	−12, −8, −4

particle-particle and particle-surface are described by the following equations:

$$U^{att}_{LJ(PP)}(r) = -\frac{A_{PP}}{6k_BT}\left[\frac{2}{r^2-4}+\frac{2}{r^2}+\ln\left(1-\frac{4}{r^2}\right)\right] \quad (11)$$

$$U^{att}_{LJ(PS)}(z) = -\frac{A_{PS}}{6k_BT}\left[\frac{1}{z-1}+\frac{1}{z+1}+\ln\left(\frac{z-1}{z+1}\right)\right] \quad (12)$$

Here, A_{pp} and A_{ps} are the Hamaker constants for the interactions between a pair of nanoparticles, and that between nanoparticle–surface, respectively. The effective interactions in Eqs. (11) and (12) are obtained by integrating the Lennard-Jones attractive interactions of the constituting atoms of a nanoparticle and the surface, respectively (Hamaker, 1937). The Hamaker constant depends on the nature of the two interacting materials, intervening medium and its ionic concentration. Here, they are held fixed for all the systems studied for simplicity (Carnie et al., 1994). We note that the Eqs. (11) and (12) are singular at $r=2$ and $z=1$, respectively. This leads to conditions where two particles might overlap or a particle penetrates the surface. To avoid this situation, we also consider the contribution of the repulsive part of the effective Lennard-Jones potential (Everaers and Ejtehadi, 2003). The repulsive interaction between a pair of nanoparticle and that between a nanoparticle and the surface are given in Eqs. (13) and (14), respectively.

$$U^{rep}_{LJ(PP)}(r) = \frac{A_{PP}}{37800k_BT}\frac{\sigma^6}{r}\left[\frac{r^2-14r+54}{(r-2)^7}+\frac{r^2+14r+54}{(r+2)^7}-\frac{2(r^2-30)}{(r)^7}\right] \quad (13)$$

$$U^{rep}_{LJ(PS)}(z) = \frac{A_{PS}}{k_BT}\left[\frac{\sigma^6}{7560}\left(\frac{7-z}{(z-1)^7}+\frac{7+z}{(z+1)^7}\right)\right] \quad (14)$$

We specifically set the exclusion thickness $\sigma=0.1$ such that neither nanoparticles overlap nor they penetrate the surface, due to the steric exclusion. The Hamaker constants as obtained from the Lifshitz theory (Bergstrom et al., 1999; Hough and White, 1980; Senden and Drummond, 1995) are listed in Table 1, which are used in this study.

All the calculations in this work are done in reduced units. The simulations are conducted at a reduced temperature $\overline{T}=1$, corresponding to an actual temperature of 298 K. The equations of motions are integrated using the Verlet algorithm (Frenkel and Smith, 2001) with a time step of $0.003\tau_0$, where $\tau_0 = a\sqrt{\frac{m}{k_BT}}$ is the unit of time. Systems are equilibrated for 10^8 steps followed by 10^7 steps of production run. The cut-off distance for the effective Lennard-Jones interaction is $9a$ and for the electrostatic interaction it is $3k^{-1}$, so as to allow all the interactions to die out significantly within half of the simulation box. All the simulations are performed using the LAMMPS (Large-scale Atomic/Molecular Massively Parallel Simulator) package (Plimpton, 1995).

3. Results and discussion

First, we investigate the generic behavior of the electrostatic and effective Lennard-Jones interactions between two silica nanoparticles, and between a silica nanoparticle and a cellulose surface in an aqueous medium. The electrostatic potential of silica – silica and silica – cellulose interactions are calculated using the zeta potentials, as discussed in Section 2. Fig. 2 shows the total interaction energy as a function of distance for different ka values. This accounts for both the effective Lennard-Jones and electrostatic interactions. In this case study, we used $\Psi_P = -40$ mV and $\Psi_S = -12$ mV for the calculation of the electrostatic interactions. The silica–silica interaction energy (U_{PP}), which is the summation of Eqs. (5), (11) and (13), is shown in Fig. 2a. The U_{PP} shows that the energy between two particles monotonically increases as they come closer, which is an indication of repulsive interaction at close proximity. The interaction energy however decays significantly with increasing distance and it attains a negligible value at a distance $r=4$. Interestingly, the U_{PP} is not much influenced by the screening length, as the change in interactions with ka is

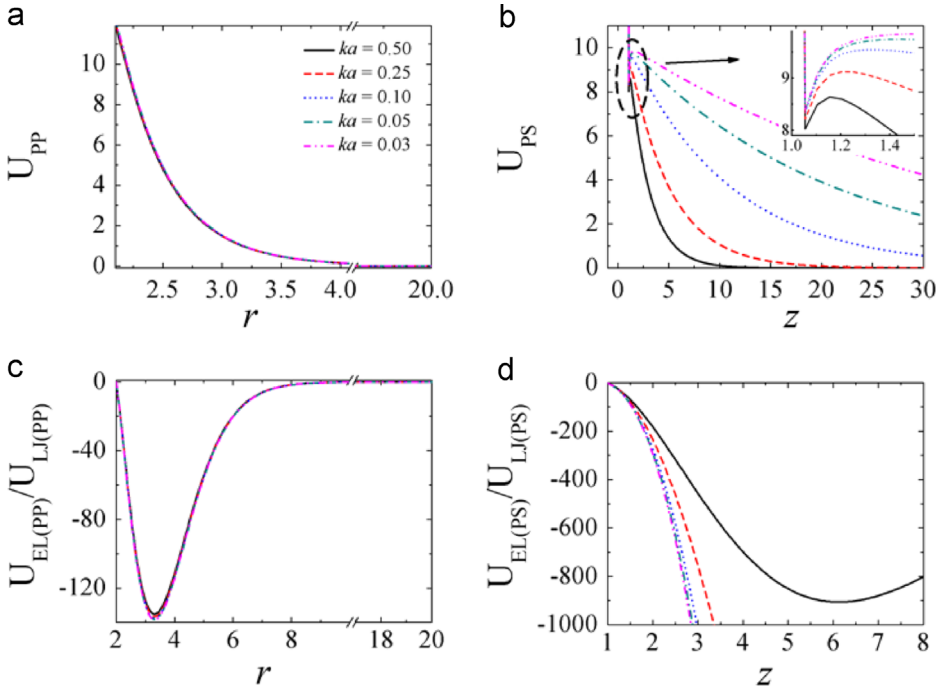

Fig. 2. Total interaction energies between (a) two silica nanoparticles U_{PP} as a function of the distance between their centers r and, (b) a silica nanoparticle and the cellulose surface U_{PS} as a function of the distance between the nanoparticle's center and the cellulose surface z. Inset shows a zoomed image of the highlighted region of the interaction energies. The (c) and (d) represent the ratio of the electrostatic to the effective Lennard-Jones interaction energies for particle–particle and particle–surface respectively. For all the cases, $\Psi_P = -40$ mV and $\Psi_S = -12$ mV.

insignificant. Similarly, the interaction energy between a silica nanoparticle and the cellulose surface (U_{PS}), which is the summation of Eqs. (6), (12) and (14), is shown in Fig. 2b, for different ka values. While U_{PS} gradually increases with decrease in the particle-surface distance, it drops visibly at a very small distance from the surface. The drop in the U_{PS} near the surface increases with decreasing ka. Thus, when a particle comes close to a surface the energy shows different behavior for varying ka values. Unlike the silica–silica interaction, here the decay of interaction strength with increasing distance strongly depends on the ka. As ka decreases, the U_{PS} decays slowly. For example, the interaction does not die out significantly even at a distance of $z=60$ for $ka \leq 0.05$. Fig. 2c and d presents the ratio of the electrostatic to the effective Lennard-Jones energies for the particle–particle and surface–particle interactions, respectively. The magnitude of the ratio is much greater than one for both the cases. This indicates that the electrostatic interaction dominates over the effective Lennard-Jones interaction. The negative sign of the ratio is due to the fact that the effective Lennard-Jones interaction is negative while the effective electrostatic interaction is positive. Therefore, we infer that the adsorption process is mainly governed by the electrostatic interactions between a pair of nanoparticles and that between nanoparticles and the surface. Further, we investigate the interplay between the particle–particle and particle–surface electrostatic interactions. The ratio of the electrostatic energy for the nanoparticle–surface to that of nanoparticle–nanoparticle interactions is shown in Fig. 3. It is clearly evident that the ratio, $U_{EL(PS)}/U_{EL(PP)}$, is below unity for small distances, which is typically seen for $r<2.25$ or $z<1.25$. This implies that the nanoparticle–nanoparticle electrostatic energy is higher than that of the nanoparticle–surface electrostatic energy at short distances. The ratio further decreases as ka decreases (near $z=1.0$), as shown in the inset of Fig. 3. As a consequence, we anticipate that nanoparticles would tend to accumulate near the surface as ka decreases, in order to minimize the system's energy.

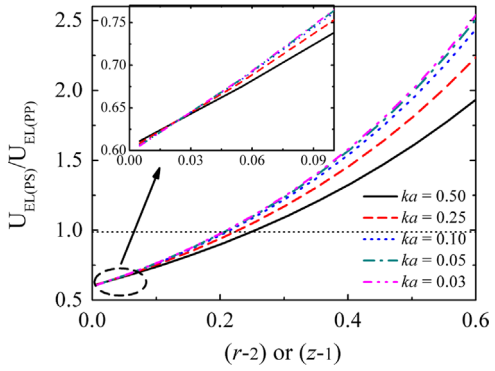

Fig. 3. Ratio of the electrostatic energy due to interaction between a silica nanoparticle and the cellulose surface to that between two silica nanoparticles. The x-axis represent the closest surface to surface separation distance $(r-2)$ in case of the nanoparticle–nanoparticle interaction, and the distance between the cellulose surface and a nanoparticle surface $(z-1)$ in case of nanoparticle–surface interaction. The ratio is evaluated at equal $(r-2)$ and $(z-1)$. The inset shows the zoomed values at very close distances. For all the cases, $\Psi_P=-40$ mV and $\Psi_S=-12$ mV.

Below, we present the Brownian dynamics simulation results in two different subsections. In Subsection 3.1, the adsorption of nanoparticles from their bulk suspension is discussed. Subsection 3.2 represents the structure and dynamics of adsorbed nanoparticles in the monolayer.

3.1. Nanoparticles adsorption on the surface

Here, we focus on nanoparticles adsorption on the surface. We have analyzed the nanoparticles density as a function of the perpendicular distance above the surface. The z-density profile (ρ_z) is defined as the local density of nanoparticles at a distance z above the surface, normalized by the global density of nanoparticles in the system. Thus, the z-density profile is written as

$$\rho_z = \frac{\langle n(z) \rangle}{L_x L_y \Delta z} \Big/ \frac{N_{box}}{V_{box}}. \tag{15}$$

Here, L_x and L_y correspond to the box length along x- and y-directions, respectively. The $n(z)$ is the number of nanoparticles within a distance between z and $z+\Delta z$ above the surface along the z-direction, We choose $\Delta z=0.1$ in this study. The N_{box} and V_{box} are total number of particles in the system and total volume, respectively. Fig. 4 shows the z-density profile for $ka=0.25$ and 0.1, for four different volume fractions (ϕ) of nanoparticles in the system. Fig. 4a indicates that nanoparticles density near the surface is very low, in comparison to that far away from the surface. Therefore, particles are repelled away from the surface as shown by the cartoon in the inset. The ρ_z reaches a value close to one, at a very large distance from the surface. This trend is independent of the particles volume fraction. On the other hand, a strong peak is observed at around $z=1$ for $ka=0.1$, as shown in the Fig. 4b. This implies a layer of nanoparticles near the surface, as depicted by the cartoon in the inset. The peak height increases as the nanoparticles volume fraction increases. This indicates that the nanoparticles density in the layer increases as particles bulk volume fraction in the system increases. We, therefore, identify a crossover from the suspension to the adsorption of nanoparticles on the surface as ka decreases. The transition, which is observed at $ka=0.1$, seems to be independent of the particles volume fraction. Further the adsorption of nanoparticles for $ka<0.1$ is investigated for wide

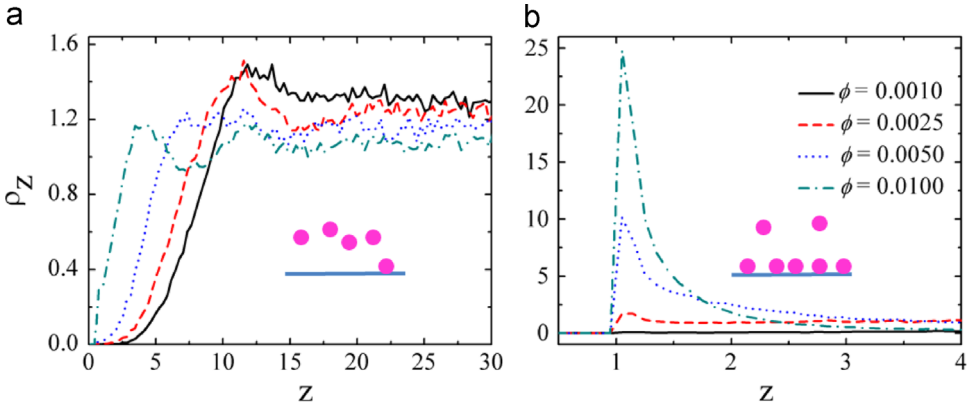

Fig. 4. The z-density profile of nanoparticles for (a) $ka=0.25$ (b) $ka=0.1$, for $\Psi_P=-40$ mV and $\Psi_S=-12$ mV. The insets in (a) and (b) show a schematic representation of the distribution of particles over the surface.

range of their volume fraction. Fig. 5a–d shows the BD snapshots of adsorbed nanoparticles at different volume fractions for $ka=0.05$, and the corresponding ρ_z functions are shown in Fig. 5e. Nanoparticles within a distance of $z=2.0$ from the surface are considered to be adsorbed, and are shown in Fig. 5. It is evident from the snapshots that the number of nanoparticles adsorbed on the surface increases with increase in the bulk volume fraction of nanoparticles. Thus, the peak height of the ρ_z increases as ϕ increases. But the peak position remains fixed as seen in Fig. 5e. We note that nanoparticles are adsorbed on a single layer. In all the cases, multi layers are not seen, which is due to the fact that the adsorbed nanoparticles repel the non-adsorbed nanoparticles.

To further understand the adsorption mechanism of nanoparticles on the surface, we have calculated the potential of mean force for the particle–particle (PMF_{PP}) and the particle–surface (PMF_{PS}) interactions. The potential of mean force, in the reduced form for a particle–particle interaction is given by $PMF_{PP} = -\ln(g_{bulk}(r))$, and that for particle–surface interaction is $PMF_{PS} = -\ln(\rho_z)$ (Patra and Singh, 2013). Here $g_{bulk}(r) = \frac{\langle N_b(r,r+\Delta r)\rangle}{4\pi r^2 \Delta r} / \frac{N_{box}}{V_{box}}$, is the nanoparticle radial distribution function, which is calculated using $\Delta r = 0.1$. The ρ_z is the z-density profile as described in Eq. (15). The Fig. 6a and b shows the potential of mean force for particle–particle and particle–surface interactions respectively, for $\phi=0.005$. The PMF_{PP} represents repulsive interaction between a pair of nanoparticles, as it monotonically decreases as a function of the distance between them. The nature of interaction remains repulsive as ka varies, as shown in Fig. 6a. On the other hand, the PMF_{PS} is strongly dependent on ka. For $ka=0.5$ and 0.25, it represents repulsive interaction between the surface and nanoparticles. As ka decreases, the interaction becomes attractive as the PMF_{PS} shows a minimum at a distance of the order of nanoparticle's radius. This crossover from the repulsive to the attractive interaction is identified at $ka=0.1$. As the ka decreases beyond 0.1, the strength of attraction increases as shown in Fig. 6b. Therefore, the potential of mean force suggests the adsorption of particles for $ka \lesssim 0.1$. This observation is in agreement with Fig. 4 where particles are shown to adsorb for $ka \lesssim 0.1$. Interestingly, the minimum in the PMF_{PS} is followed by an energy barrier as shown in Fig. 6b for $ka \lesssim 0.1$. The height of the barrier increases as ka decreases. It has a significant impact on the kinetics of the adsorption process. We anticipate a slower rate of adsorption of particles for higher energy barrier. Further, the surface coverage is expected to be higher for higher energy barrier, as it corresponds to a deeper energy minimum. These effects are directly observed in simulations by calculating the surface coverage with respect to time, which are presented in the following part of the manuscript.

The time evolution of the surface coverage $\theta(\bar{t})$ is measured to quantify the maximum amount of nanoparticles adsorbed on the surface for different screening lengths and their bulk concentration. The bulk equilibrium configuration of nanoparticles is generated by conducting simulations for 10^7 steps in the absence of surfaces. Then we bring two surfaces at the bottom and top of the simulation box along the z-axis, and record the nanoparticles adsorbed on the surface as a function of time. Here, the surface coverage is defined as the ratio of projected area of absorbed

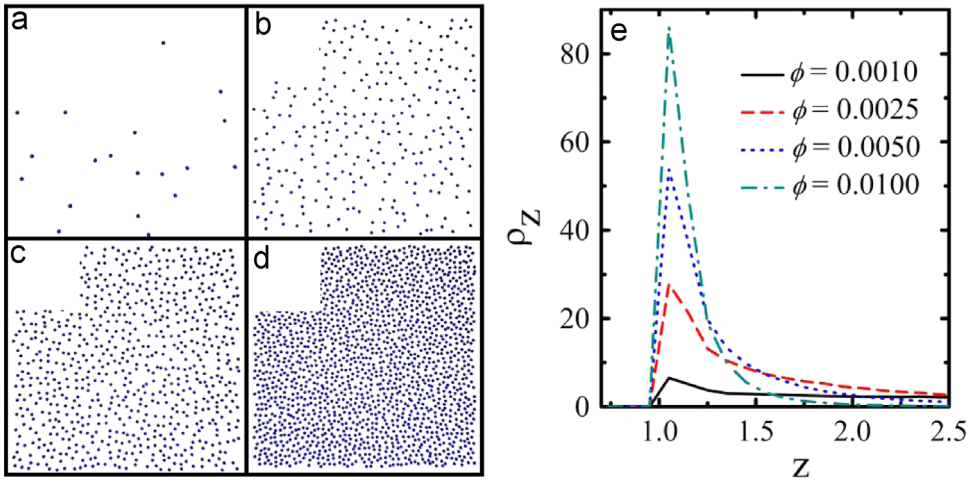

Fig. 5. The BD snapshots of nanoparticles adsorbed on the surface for $ka=0.05$, $\Psi_P=-40$ mV and $\Psi_S=-12$ mV, for (a) $\phi=0.001$ (b) $\phi=0.0025$ (c) $\phi=0.005$ and (d) $\phi=0.01$. The z-density profiles of nanoparticles are shown in (e) for the four cases.

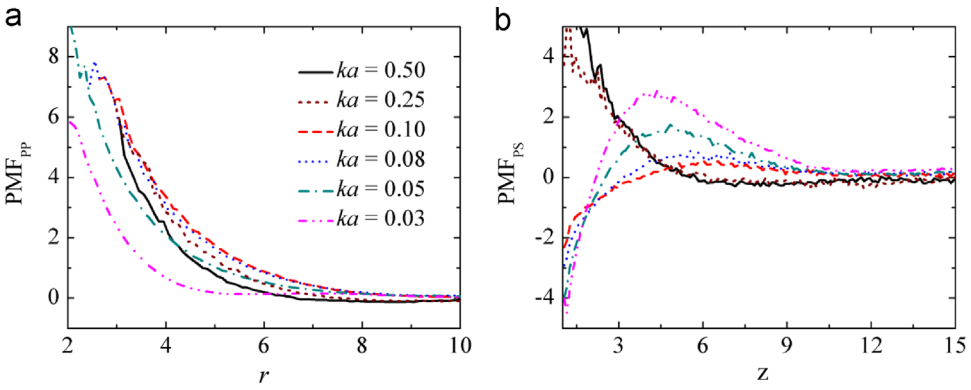

Fig. 6. Potential of mean force between (a) particle–particle and (b) particle–surface for $\phi=0.005$. All the plotted data are for $\Psi_P=-40$ mV and $\Psi_S=-12$ mV.

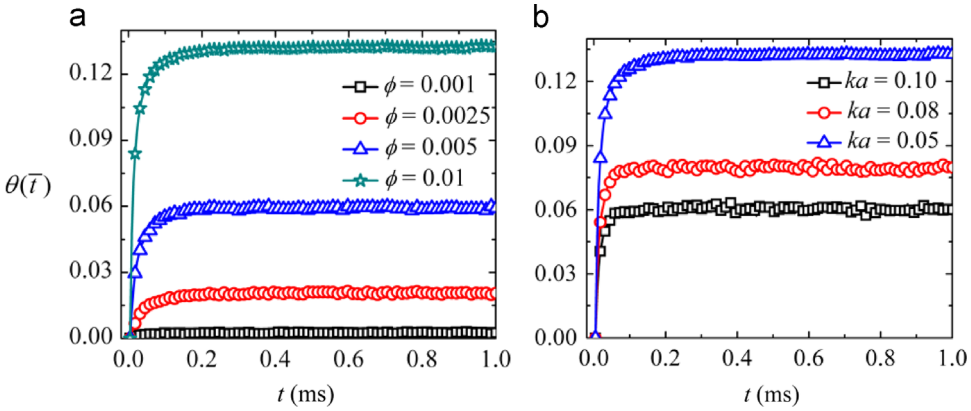

Fig. 7. The surface coverage is plotted as a function of time for (a) ka=0.05 and (b) ϕ=0.01, for Ψ_P= −40 mV and Ψ_S= −12 mV.

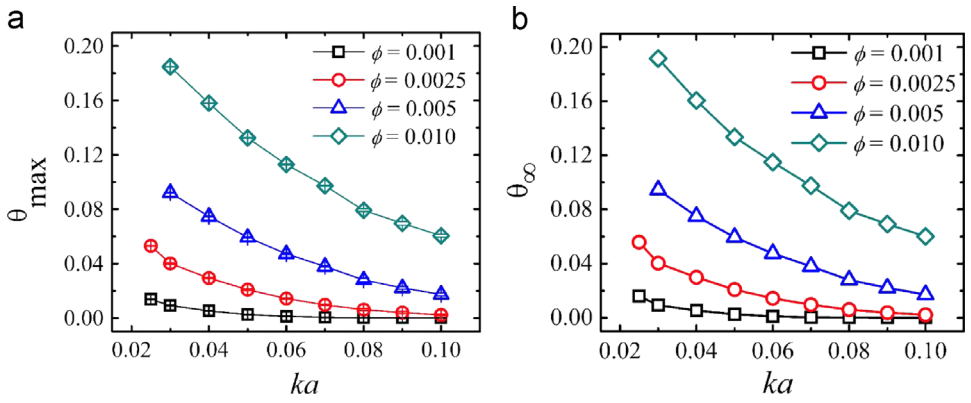

Fig. 8. (a) The maximum surface coverage θ_{max}, and (b) the equilibrium surface coverage θ_∞, which is calculated from Eq. (17), are shown as a function of ka. Both correspond to Ψ_P= −40 mV and Ψ_S= −12 mV.

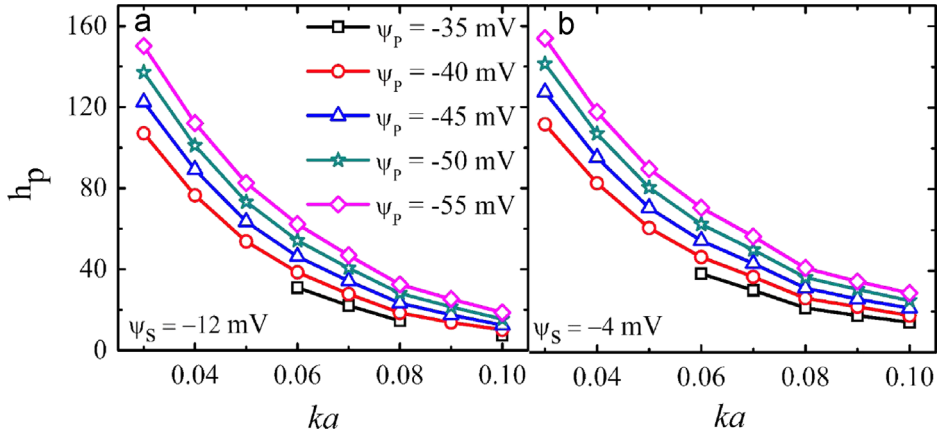

Fig. 9. The peak height, h_p of the z-density profile is shown as a function of ka at ϕ=0.005 for (a) Ψ_S= −12 mV and (b) Ψ_S= −4 mV.

particles to the total area of the surface:

$$\theta(\bar{t}) = n_{ad}(\bar{t})\pi\frac{\bar{a}^2}{A_{Surface}}. \tag{16}$$

where $n_{ad}(\bar{t})$ represents the number of nanoparticles on the surface at a time $\bar{t}$. The $A_{surface}$ is the area of the surface. Fig. 7a shows the surface coverage as a function of time for ka=0.05 for various values of ϕ. Similarly, Fig. 7b shows the surface coverage for ϕ=0.01 for various ka values. Initially, the surface coverage increases very rapidly with time and then reaches a saturation (plateau). As ka decreases, it takes more time to reach the plateau region. Similar, as ϕ increases, it takes more time to reach the plateau region. The cause for such a behavior is due to barrier in the PMF_{PS} as explained in Fig. 6b. We have also estimated the maximum surface coverage θ_{max} as the average of the data points in the plateau region. The maximum surface coverage as a function of ka for different ϕ values is obtained as shown in Fig. 8a. Further, the equilibrium surface coverage (θ_∞) is defined as the amount of nanoparticles adsorbed on the surface in an infinite time. According to the asymptotic power law (Schaaf et al., 1991)

$$\theta_\infty - \theta(\bar{t}) \sim \bar{t}^{-2/3}. \tag{17}$$

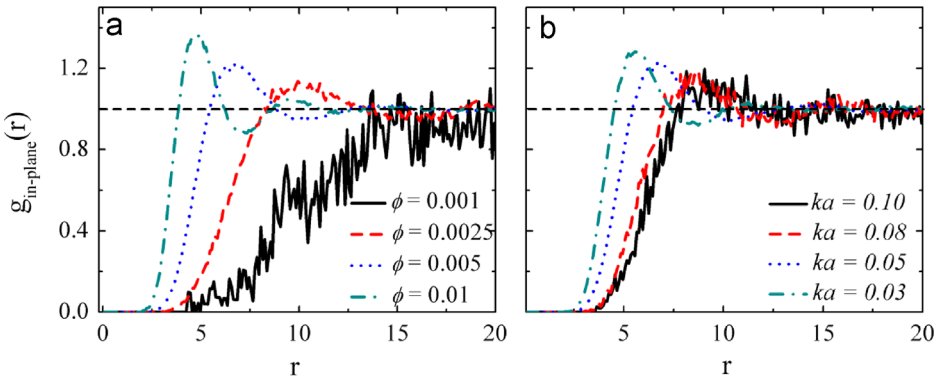

Fig. 10. Plot of the in-plane radial distribution function for (a) $ka=0.05$ and (b) $\phi=0.005$. Both correspond to $\Psi_P=-40$ mV and $\Psi_S=-12$ mV.

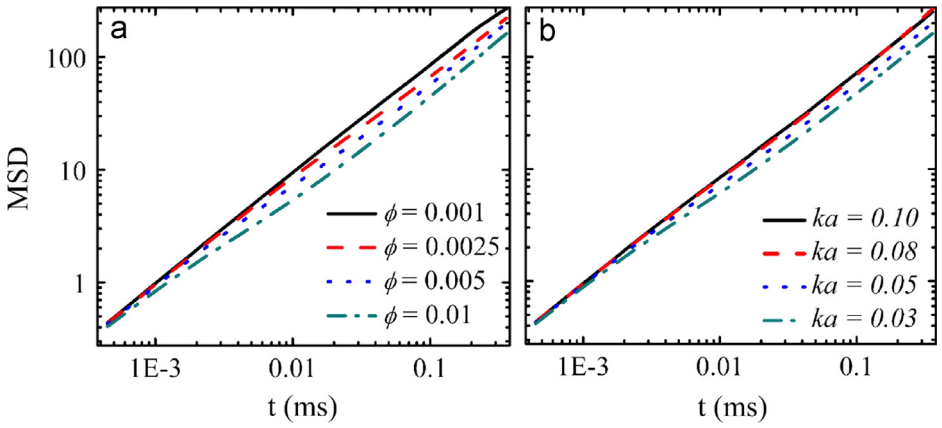

Fig. 11. The mean squared displacement (MSD) of a nanoparticle in the adsorbed monolayer is plotted as a function of time for (a) $ka=0.05$, and (b) $\phi=0.005$. Both correspond to $\Psi_P=-40$ mV and $\Psi_S=-12$ mV.

Here, $\bar{t}$ is the time in reduced units. The above expression is fitted to the data of $\theta(\bar{t})$ vs $\bar{t}^{-2/3}$ to obtain θ_∞. Fig. 8b shows the θ_∞ as a function of ka for different ϕ values. It is observed that θ_{max} and θ_∞ are nearly same. It further signifies that the simulation time is sufficient to capture the maximum amount of nanoparticles adsorbed for a given system. The surface coverage increases exponentially as ka decreases, as seen in Fig. 8. Further, it increases as ϕ increases for a constant ka. This observation is in agreement with the experimental results (Mahouche-Chergui et al., 2014). Therefore, high value of ϕ and low value of ka are good for obtaining better adsorption of nanoparticles on the surface.

The above case study is conducted for a particular combination of the nanoparticle and surface potentials i.e. $\Psi_P=-40$ mV and $\Psi_S=-12$ mV. Similar studies are repeated for various ka values and at $\phi=0.05$, and combinations of Ψ_P and Ψ_S as given in Table 2. The z-density profile is estimated for all the cases. The peak heights of the z-density profiles (h_p) are shown in Fig. 9 as a function of ka, to qualitatively compare the amount of nanoparticles adsorbed on the surface for different combinations of Ψ_P and Ψ_S. Fig. 9 indicates that the height of the peak increases with the decrease in the magnitude of Ψ_S for a particular Ψ_P value. It also indicates that the height of the peak increases with the increase in magnitude of Ψ_P for a fixed Ψ_S. The decrement in the magnitude of Ψ_S reduces the repelling force between the surface and particles. On the other hand, the increment in the magnitude of Ψ_P increases the repelling forces between particles. Hence, the adsorption of nanoparticles on the surface increases in both the cases.

3.2. Structure and dynamics of nanoparticles in the adsorbed monolayer

All the above analysis confirms that there is an adsorbed monolayer on the surface for $ka \leq 0.1$. In this section, we study the effects of screening length and nanoparticles volume fraction on the structure and dynamics of the adsorbed monolayer. The in-plane radial distribution function $g_{in\text{-}plane}(r)$ is calculated, which is defined as

$$g_{in-plane}(r) = \frac{\langle N(r, r+\Delta r)\rangle}{2\pi r \Delta r} \Big/ \frac{N_{ad}}{A_{Surface}}. \tag{18}$$

Here $\langle N(r, r+\Delta r)\rangle$ is the average number of nanoparticles in a circular bin between two distances r and $r+\Delta r$ from the center of mass of a nanoparticle in the adsorbed monolayer (2D). We choose, $\Delta r=0.1$ in this study. The radial distribution function is shown in Fig. 10a for $ka=0.05$, for different volume fraction of nanoparticles. The $g_{in\text{-}plane}(r)$ reaches to unity from below for a very low volume fraction, $\phi=0.001$. This behavior indicates that nanoparticles are distributed randomly in the monolayer, similar to a gas-like state. As ϕ increases, we observed a distinct peak in the $g_{in\text{-}plane}(r)$. Further, the position of the peak shifts to the left from $r=10.5$ to 6.5 as ϕ increases from 0.0025 to 0.005. This implies that the average distance between two neighboring nanoparticles decreases as ϕ increases. Also, the peak height of the $g_{in\text{-}plane}(r)$ increases as ϕ increases. This indicates a denser arrangement of nanoparticles in the monolayer. Similarly, Fig. 10b presents the radial distribution function for $\phi=0.005$, for varying ka. Here also we observe a single peak in the radial distribution function. The peak position shifts to the left as ka decreases. For

example the peak position changes from $r=8.5$ to 7.85 as ka decreases from 0.1 to 0.08, leading to a shorter distance between a pair of nanoparticles. The peak height of the $g_{\text{in-plane}}(r)$ also increases as ka decreases. This indicates a denser arrangement of particles as ka decreases. However, there are no specific crystal-like arrangement among the nanoparticles for all the cases. Usually, nanoparticles are in an ordered state if there exist a split in the second peak of their radial distribution function (Miyahara et al., 2004). In our case, we do not observe any such split; in fact a pronounced second peak is not present in any of the cases. This is a signature of liquid-like structure. We, therefore, observe a transition from a gas-like structure to a liquid-like structure in the adsorbed monolayer as the nanoparticles volume fraction increases.

Further the dynamics of the nanoparticles in the monolayer is investigated by calculating the in-plane mean squared displacement (MSD) of the adsorbed nanoparticles as a function of time. The MSD is defined as

$$MSD(\bar{t}) = \frac{1}{N_m}\sum_{i=1}^{N_m}\left\langle \left[r_i(\bar{t}) - r_i(0)\right]^2 \right\rangle. \tag{19}$$

where $r_i(\bar{t})$ is the position vector of the nanoparticle 'i' at a time '$\bar{t}$' and N_m is the total number of nanoparticles in the monolayer. Fig. 11 shows the MSD of a nanoparticle as a function of time. The MSD of a nanoparticle in the adsorbed layer increases as ϕ decreases, as shown in Fig. 11a. This is due to their low density in the adsorbed monolayer. On the other hand, when ϕ further increases more nanoparticles adsorb on the surface and the movement of nanoparticles gets restricted. Similarly, Fig. 11b indicates that the MSD decreases as ka decreases. As ka decreases, the range of electrostatic interaction increases causing slower mobility of the particles. Moreover, the mean square displacement of a particles is related to its dynamical time as $MSD(\bar{t}) \sim \bar{t}^{\mu}$ (Patra et al., 2012). In case of normal diffusion $\mu=1$ and it is less than one for subdiffusive particles. In all the MSD plots shown in Fig. 11, we find that the μ varies from 0.91 to 0.97. Hence, we conclude that nanoparticles in the adsorbed monolayer undergo subdiffusive motion.

4. Conclusions

In this work, we have studied the suspension and adsorption of silica nanoparticles on a cellulose surface using Brownian dynamics simulations. The effective Lennard-Jones and electrostatic interactions for silica–silica and silica–cellulose are calculated in an aqueous medium based on the DLVO theory. These interactions are influenced by the concentration of the suspension. The electrostatic interaction dominates over the effective Lennard-Jones interaction, and determines the adsorption or suspension of nanoparticles over a surface. Our analysis has also emphasized the interplay between the nanoparticle–nanoparticle and the nanoparticle–surface electrostatic interactions. The influence of the nanoparticles volume fraction (ϕ) and the Debye screening length (k^{-1}) on their suspension and adsorption is systematically studied. A crossover from the suspension to the adsorption of nanoparticles is identified as ka decreases. Nanoparticles remain suspended in the bulk medium and non-adsorbed for $ka > 0.1$. However, the adsorption of nanoparticles on the surface is observed for $ka \leq 0.1$. The crossover is independent of the bulk concentration of nanoparticles in the medium. Thus, our work has identified the adsorption of negatively charged silica nanoparticles on a negatively charged cellulose surface, and presented an explanation for such an adsorption behavior. The adsorption mechanism is explained using potential of mean force. It is observed that the amount of nanoparticles adsorbed depends on their bulk concentration. As nanoparticles bulk concentration increases, their adsorption on the surface also increases. This leads to an increase in the surface coverage, and decrease in the mobility of nanoparticles in the adsorbed monolayer. The distribution of nanoparticles in the adsorbed monolayer is also investigated. The monolayer consists of nanoparticles in a disordered arrangement. Further a transition from a gas-like structure to a liquid-like structure of the adsorbed nanoparticles in the monolayer is shown as their bulk volume fraction increases. The impact of nanoparticles zeta potential and surface zeta potential on the adsorption of nanoparticles over a surface is demonstrated in this numerical investigation.

Acknowledgments

This work is supported by the Unilever R&D, Bangalore. The computational resources are provided by the HPC cluster of the Computer Center (CC), Indian Institute of Technology Kanpur. We thank Nisha Masawan for her help in measuring the pH of silica solutions.

Appendix A. Supplementary material

Supplementary data associated with this article can be found in the online version at http://dx.doi.org/10.1016/j.ces.2015.11.026.

References

Adamczyk, Z., Jaszczo´łt, K., Michna, A., Siwek, B., Szyk-Warszyn´ska, L., Zembala, M., 2005. Irreversible adsorption of particles on heterogeneous surfaces. Adv. Colloid Interface Sci. 118, 25.
Adamczyk, Z., Siwek, B., Weron´ski, P., Musiał, E., 2002. Irreversible adsorption of colloid particles at heterogeneous surfaces. Appl. Surf. Sci. 196, 250.
Adamczyk, Z., Siwek, B., Zembala, M., 1992. Kinetics of localized adsorption of particles on homogeneous surfaces. J. Colloid Interface Sci. 151, 351.
Adamczyk, Z., Szyk, L., 2000. Kinetics of irreversible adsorption of latex particles under diffusion-controlled transport. Langmuir 16, 5730.
Adamczyk, Z., Weronski, P., Musial, E., 2001. Colloid particle adsorption on partially covered (random) surfaces. J. Colloid Interface Sci. 241, 63.
Bergstrom, L., Stemme, S., Dahlfors, T., Arwin, H., Odberg, L., 1999. Spectroscopic ellipsometry characterisation and estimation of the Hamaker constant of cellulose. Cellulose 6, 1.
Bowen, W.R., Sharif, A.O., 1999. Long-range electrostatic attraction between like-charge spheres in a charged pore. Nature 402, 841.
Brewer, D.D., Tsapatsis, M., Kumar, S., 2010. Dynamics of surface structure evolution in colloidal adsorption: charge patterning and polydispersity. J. Chem. Phys. 133, 034709.
Butler, J.C., Angelini, T., Tang, J.X., L.Wong, G.C., 2003. Ion multivalence and like-charge polyelectrolyte attraction. Phys. Rev. Lett. 91, 028301.
Carnie, S.L., Chan, D.Y.C., Stankovich, J., 1994. Computation of forces between spherical colloidal particles: nonlinear Poisson–Boltzmann theory. J. Colloid Interface Sci. 165, 116.
Chaikin, Y., Kedem, O., Raz, J., Vaskevich, A., Rubinstein, I., 2013. Stabilization of metal nanoparticle films on glass surfaces using ultrathin silica coating. Anal. Chem. 85, 10022.
Crocker, J.C., Grier, D.G., 1996. When like charges attract: the effects of geometrical confinement on long-range colloidal interactions. Phys. Rev. Lett. 77, 1897.
Dünweg, B., Paul, W., 1991. Brownian dynamics simulations without gaussian random numbers. Int. J. Mod. Phys. C 2, 817.
Everaers, R., Ejtehadi, M.R., 2003. Interaction potentials for soft and hard ellipsoids. Phys. Rev. E 67, 041710.
Feder, J., 1980. Random sequential adsorption. J. Theor. Biol. 87, 237.
Frenkel, D., Smith, B., 2001. Understanding Molecular Simulation: From Algorithms to Applications. Academic press, Inc., Orlando, FL, USA.
Gallardo, A., Grandner, S., Almarza, N.G., Klapp, S.H.L., 2012. Theory of repulsive charged colloids in slit-pores. J. Chem. Phys. 137, 014702.
Gray, J.J., Bonnecaze, R.T., 2001. Adsorption of colloidal particles by Brownian dynamics simulation: kinetics and surface structures. J. Chem. Phys. 114, 1366.
Gray, J.J., Chiang, B., Bonnecaze, R.T., 1999. Origin of anomalous multibody interactions. Nature 402, 750.
Grier, D.G., 1998. A surprisingly attractive couple. Nature 393, 621.

Hamaker, H.C., 1937. The London-van der Waals attraction between spherical particles. Physica 4, 1058.
Hanarp, P., Sutherland, D.S., Gold, J., Kasemo, B., 2003. Control of nanoparticle film structure for colloidal lithography. Colloids Surf. A 214, 23.
Hattori, H., 2001. Anti-reflection surface with particle coating deposited by electrostatic attraction. Adv. Mater. 13, 51.
Hough, D.B., White, L.R., 1980. The calculation of Hamaker constants from Lifshitz theory with applications to wetting phenomena. Adv. Colloid Interface Sci. 14, 3.
Jeon, S.I., Andrade, J.D., 1991. Protein-surface interactions in the presence of polyethylene oxide II. Effect of protein size. J. Colloid Interface Sci. 142, 159.
Jeon, S.I., Lee, J.H., Andrade, J.D., Gennes, P.G.D., 1991. Protein-surface interactions in the presence of polyethylene oxide I. Simplified theory. J. Colloid Interface Sci. 142, 149.
Joannopoulos, J.D., Meade, R.D., Winn, J.N., 1995. Photonic Crystals. Princeton University Press, Princeton, NJ, USA.
Johnson, C.A., Lenhoff, A.M., 1996. Adsorption of charged latex particles on mica studied by atomic force microscopy. J. Colloid Interface Sci. 179, 587.
Juillerat, F., Solak, H.H., Bowen, P., Hofmann, H., 2005. Fabrication of large-area ordered arrays of nanoparticles on patterned substrates. Nanotechnology 16, 1311.
Kasemo, B., Johansson, S., Persson, H., Thormahlen, P., Zhdanov, V.P., 2000. Catalysis in the nm-regime: manufacturing of supported model catalysts and theoretical studies of the reaction kinetics. Catalysis 13, 43.
Kulkarni, P., Sureshkumar, R., Biswas, P., 2003. Multiscale simulation of irreversible deposition in presence of double layer interactions. J. Colloid Interface Sci. 260, 36.
Larsen, A.E., Grier, D.G., 1997. Like-charge attractions in metastable colloidal crystallites. Nature 385, 230.
Lee, C.K., Hua, C.C., 2010. Nanoparticle interaction potentials constructed by multiscale computation. J. Chem. Phys. 132, 224904.
Liu, B.-T., Yeh, W.-D., 2010. Antireflective surface fabricated from colloidal silica nanoparticles. Colloids Surf. A 356, 145.
Magan, R.V., Sureshkumar, R., 2006. Multiscale-linking simulation of irreversible colloidal deposition in the presence of DLVO interactions. J. Colloid Interface Sci. 297, 389.
Mahouche-Chergui, S., Grohens, Y., Balnois, E., Lebeau, B., Scudeller, Y., 2014. Adhesion of silica particles on thin polymer films model of flax cell wall. Mater. Sci. Appl. 5, 953.
Miyahara, M., Watanabe, S., Gotoh, Y., Higashitani, K., 2004. Adsorption and order formation of colloidal nanoparticles on a substrate: a Brownian dynamics study. J. Chem. Phys. 120, 1525.
Miyahara, M., Watanabe, S., Higashitani, K., 2006. Modeling adsorption and order formation by colloidal particles on a solid surface: a Brownian dynamics study. Chem. Eng. Sci. 61, 2142.
Nagornyak, E., Yoo, H., Pollack, G.H., 2009. Mechanism of attraction between like-charged particles in aqueous solution. Soft Matter 5, 3850.
Nakanishi, K., Sakiyama, T., Imamura, K., 2001. On the adsorption of proteins on solid surfaces, a common but very complicated phenomenon. J. Biosci. Bioeng. 91, 233.
Nepal, D., Onses, M.S., Park, K., Jespersen, M., Thode, C.J., Nealey, P.F., Vaia, R.A., 2012. Control over position, orientation, and spacing of arrays of gold nanorods using chemically nanopatterned surfaces and tailored particle–particle–surface interactions. Acs Nano 6, 5693.
Oberholzer, M.R., Wagner, N.J., Lenhoff, A.M., 1997. Grand canonical Brownian dynamics simulation of colloidal adsorption. J. Chem. Phys. 107, 9157.
Patra, T.K., Hens, A., Singh, J.K., 2012. Vapor–liquid phase coexistence and transport properties of two-dimensional oligomers. J. Chem. Phys. 137, 084701.
Patra, T.K., Katiyar, P., Singh, J.K., 2015. Substrate directed self-assembly of anisotropic nanoparticles. Chem. Eng. Sci. 121, 16.
Patra, T.K., Singh, J.K., 2013. Coarse-grain molecular dynamics simulations of nanoparticle-polymer melt: dispersion vs. agglomeration. J. Chem. Phys. 138, 144901.
Patra, T.K., Singh, J.K., 2014. Localization and stretching of polymer chains at the junction of two surfaces. J. Chem. Phys. 140, 204909.
Plimpton, S.J., 1995. Fast parallel algorithms for short–range molecular dynamics. J. Comp. Phys. 117, 1.
Ravichandran, S., Talbot, J., 2000. Mobility of adsorbed proteins: a Brownian dynamics study. Biophys. J. 78, 110.
Sader, J.E., 1997. Accurate analytic formulae for the far field effective potential and surface charge density of a uniformly charged sphere. J. Colloid Interface Sci. 188, 508.
Schaaf, P., Johner, A., Talbot, J., 1991. Asymptotic behavior of particle deposition. Phys. Rev. Lett. 66, 1603.
Schneider, T., Stoll, E., 1978. Molecular-dynamics study of a three-dimensional one-component model for distortive phase transitions. Phys. Rev. B 17, 1302.
Semmler, M., Mann, E.K., Ricka, J., Borkovec, M., 1998. Diffusional deposition of charged latex particles on water–solid interfaces at low ionic strength. Langmuir 14, 5127.
Senden, T.J., Drummond, C.J., 1995. Surface chemistry and tip-sample interactions in atomic force microscopy. Colloids Surf. A 94, 29.
Squires, T.M., Brenner, M.P., 2000. Like-charge attraction and hydrodynamic interaction. Phys. Rev. Lett. 85, 4976.
Velev, O.D., Kaler, E.W., 1999. In situ assembly of colloidal particles into miniaturized biosensors. Langmuir 15, 3693.
Watanabe, S., Miyahara, M., Higashitani, K., 2005. Dynamics of order formation by colloidal adsorption onto a substrate studied with Brownian dynamics. J. Chem. Phys. 122, 104704.
Watanabe, S., Miyahara, M.T., 2010. Order formation of colloidal nanoparticles adsorbed on a substrate with friction. Adv. Powder Technol. 21, 57.
Zhang, X., Bai, R., 2002. Deposition/adsorption of colloids to surface-modified granules: effect of surface interactions. Langmuir 18, 3459.
Zhou, J., Tsao, H.-K., Sheng, Y.-J., Jiang, S., 2004. Monte Carlo simulations of antibody adsorption and orientation on charged surfaces. J. Chem. Phys. 121, 1050.
Zhou, S., 2013. Density functional analysis of like-charged attraction between two similarly charged cylinder polyelectrolytes. Langmuir 29, 12490.